REFERENCES AND NOTES

1. The series is based on the gridded monthly mean data set compiled under the sponsorship of the U.S. Department of Energy, as described in P. D. Jones *et al.*, *J. Clim. Appl. Meteorol.* **25**, 161 (1986) and updated in the references in (*7*).
2. Because this procedure maximizes the squared temporal covariance between $T^*(x,t)$ and $\bar{T}(t)$, it is equivalent to performing singular value decomposition analysis, as outlined in C. S. Bretherton, C. Smith, J. M. Wallace, *J. Clim.* **5**, 541 (1992), where $T^*(x,t)$ is the left field and $\bar{T}$ is the one-dimensional right field. If the number of spatial degrees of freedom in $T^*(x,t)$ is too large in comparison with the number of independent samples, this procedure will tend to overfit $\bar{T}(t)$, yielding an intricate pattern A^* that would not be reproducible in an independent data set [for example, see R. E. Davis, *J. Phys. Oceanogr.* **8**, 233 (1978)]. We investigated the sensitivity of $T_1(t)$ to the number of degrees of freedom in $A^*(x)$. Following T. P. Barnett and R. Preisendorfer [*Mon. Weather Rev.* **115**, 1825 (1987)], we expanded the T^* field in terms of its own empirical orthogonal functions, and we fit the N leading associated expansion coefficient time series to $\bar{T}(t)$ by the method of least squares. Within the range $N = 5$ to 10, $T_1(t)$ and $A^*(x)$ closely resemble those shown in the text, and the fraction of the variance of $\bar{T}(t)$ explained by the fit is also quite comparable. Hence, because of the spatial autocorrelation inherent in the T^* field, the effective number of spatial degrees of freedom in this particular application is only on the order of 5 to 10, so overfitting is not a problem.
3. The data are formatted on a latitude-longitude grid, so grid point values must be weighted by cosine of latitude in estimation of $\bar{T}(t)$ and computation of $T_1(t)$ from (*4*).
4. The field represented in Fig. 4 is the thickness of the layer between the 1000- and 500-hectopascal (or millibar) pressure surfaces, which is directly proportional to the mean temperature (in degrees Kelvin) of the intervening layer, which extends from the earth's surface up to a height of ~5.5 km above sea level. Gridded analyses of these fields have been produced by the National Oceanic and Atmospheric Administration (NOAA) National Meteorological Center on a daily or twice-daily basis since 1946, in support of operational numerical weather prediction.
5. If the hemispheric lower tropospheric temperature field is regressed upon $\bar{T}(t)$ instead of $T_1(t)$, the pattern is similar but biased toward positive values. A similar but somewhat weaker pattern is obtained when the lower tropospheric temperature field is regressed upon the time series of hemispheric mean lower tropospheric temperature, averaged over the area poleward of 40°N, including both land and ocean (*6*).
6. J. M. Wallace, Y. Zhang, L. Bajuk, *J. Clim.*, in press.
7. C. K. Folland, T. R. Karl, K. Ya. Vinnikov, in *Climate Change: The IPCC Scientific Assessment*, J. T. Houghton, G. J. Jenkins, J. J. Ephraums, Eds. (Cambridge Univ. Press, 1990), pp. 195–238; C. K. Folland *et al.*, in *Climate Change 1992: The Supplementary Report to the IPCC Scientific Assessment*, J. T. Houghton, B. A. Callander, S. K. Varney, Eds. (Cambridge Univ. Press, 1992), pp. 135–170; D. E. Parker, P. D. Jones, C. K. Folland, A. Bevan, *J. Geophys. Res.* **99D**, 14373 (1994).
8. K. E. Trenberth, *Bull. Am. Meteorol. Soc.* **71**, 988 (1990); ——— and J. W. Hurrell, *Clim. Dyn.* (in press); C. Deser and M. L. Blackmon, *J. Clim.* **6**, 1743 (1993); N. E. Graham, *Clim. Dyn.* **10**, 135 (1994); ——— T. P. Barnett, R. Wilde, M. Ponafer, S. Schubert, *J. Clin.* **7**, 1416 (1994); Y. Zhang, J. M. Wallace, N. Iwasaka, *ibid.*, in press; M. Latif and T. P. Barnett, *Science* **266**, 634 (1994); A. Kumar, A. Leetmaa, M. Ji, *ibid.*, p. 632.
9. J. W. Hurrell, *Science* **269**, 676 (1995).
10. T. M. L. Wigley and T. P. Barnett, in *Climate Change: The IPCC Scientific Assessment*, J. T. Houghton, G. J. Jenkins, J. J. Ephraums, Eds. (Cambridge Univ. Press, Cambridge, 1990), pp. 239–256, T. P. Barnett, M. E. Schlesinger, X. Jiang, in *Greenhouse Gas–Induced Climatic Change: A Critical Appraisal of Simulations and Observations*, M. E. Schlesinger, Ed. (Elsevier, Amsterdam, 1991), pp. 559–568; K. Hasselmann, *J. Clim.* **6**, 1957 (1993), B. D. Santer, T. M. L. Wigley, P. D. Jones, *Clim. Dyn.* **9**, 265 (1993).
11. See, for example, R. J. Charlson and T. M. Wigley, *Sci. Am.* **270**, 48 (1994).
12. Regression of $T(x,t)$ upon $\bar{A}T_1(t)$ yields $\bar{A}\langle TT_1\rangle/\bar{A}^2\langle T_1^2\rangle$. From Eq. 1, $\bar{A}^2\langle T_1^2\rangle = \bar{A}\langle\bar{T}T_1\rangle$. Hence, the regression coefficient is equivalent to $\langle TT_1\rangle/\langle\bar{T}\bar{T}T_1\rangle$, which reduces to $A/\bar{A}$.
13. We thank E. Sarachik, T. N. Palmer, I. Blade, C. B. Leovy, and an anonymous reviewer for reading an earlier version of the manuscript and offering helpful suggestions. Supported by NSF's Climate Dynamics Program under grant ATM 9215512 and by the NOAA Office of Global Programs.

13 June 1995; accepted 24 August 1995

On the Origins of Spontaneous Polarization in Tilted Smectic Liquid Crystals

Demetri J. Photinos and Edward T. Samulski*

The rapid electrooptic response of ferroelectric liquid crystals—stratified (smectic) melts exhibiting spontaneous electric polarization—makes them candidates for the next generation of electrooptic shutters and liquid crystal displays. The model advanced here suggests that polarity is indigenous to tilted smectics and that spontaneous polarization derives from the packing constraints mesogens experience, a tilt-dependent correlation of molecular conformation with orientation. First-rank orientational order parameters (C_{xx}) are nonzero with a tilt- (temperature-) dependent magnitude, and under certain packing conditions, the sign of C_{xx} varies with tilt. These results have a direct bearing on experimental observations because most ferroelectric liquid crystals exhibit a tilt-dependent spontaneous polarization and some show an inversion of the sign of the polarization.

Spontaneous polarization is the signature and defining characteristic of certain smectic phases called ferroelectric liquid crystals (FLCs). Since Meyer's seminal announcement that ferroelectricity can be realized in tilted smectics composed of chiral mesogens (*1*), it has been generally accepted that FLC attributes revolve around the subtle interplay between electric dipoles and molecular chirality (*2*). However, in modeling of idealized mesogens confined to lamellae, we found an indigenous polarity in even the simplest representation of a tilted smectic phase, one that was independent of mesogen molecular structural details (such as dipole moments and chirality). More than 20 years ago, Priest anticipated such a possibility in a formal description of the smectic-C (S_C) phase using the tensor components of the molecular mean field (*3*). Our modeling has led us to conclude (i) that spontaneous polarization originates from a statistical biasing of mesogen configurations that derives from steric interactions in stratified, tilted smectics and (ii) that its temperature dependence, including the observed inversion of the sign of the polarization in certain FLCs, is simply a consequence of molecular packing considerations.

The molecules forming the S_C phase typically consist of an elongated, aromatic (mesogenic) core linked to flexible, aliphatic chains ("tails") at both of its ends (**I** and **II** in Table 1). Because of molecular flexibility, the molecular symmetry is understood in the statistical or time-averaged sense. There is spatial segregation in the S_C phase along the smectic layer normal Z: core-rich zones alternate with chain-rich ones (Fig. 1). A chiral center in the mesogen (**II**) results in an incompletely averaged electric dipole component $\mu_\perp$ transverse to the mesogenic core that contributes to an electric polarization along the C_2 axis (X axis) of the tilted phase: $P_X \propto \Sigma\mu_\perp$. Meyer and his co-workers used symmetry arguments suggesting that chirality and transverse dipoles are sufficient to give rise to ferroelectricity (*1*), but these arguments do not permit the evaluation of the polarization P_X because they do not refer to any particular mechanism by which the polar order develops. Several such mechanisms have been proposed over the last two decades, but all of them invoke ad hoc constraints or parameters to affect polarization. These include a binding-site model that biases rotations of a chiral mesogen's "zig-zag" contour, thereby generating a nonzero $\mu_\perp$ (*4*), weighted mesogen conformational statistics that manufacture a temperature-dependent polarization of variable sign (*5*), and a model with multiple transverse molecular axes circumscribed to mimic different degrees of biased mesogen rotation (*6*). This report demonstrates that a generic representation of a statistically twofold-symmetric mesogen (for example, an idealization of the apolar, achiral mesogen **I**) together with the ordering constraints imposed on it by the S_C phase give rise to nonzero, first-rank polar order parameters.

Figure 2, A and B, illustrates two dispositions of a flexible primitive mesogen—a three-segment representation of the real mesogen—confined within a smectic layer. Both dispositions are compatible with strat-

---

D. J. Photinos, Department of Physics, University of Patras, Patras 26100, Greece.
E. T. Samulski, Department of Chemistry, University of North Carolina, Chapel Hill, NC 27599-3290.

*To whom correspondence should be addressed.

ification (7) and both will evidence indigenous polarity (of opposite signs). The tail segments can be rotated (ϕ_i = 0° or 180°, i = 1, 2) about the core segment to generate planar conformations. Additionally, if the two states of ϕ_i are equally probable, then both the y_0z_0 plane (Fig. 2C) and the x_0z_0 plane are also statistical symmetry planes of the primitive mesogen, that is, equally probable conformers confer D_{2h} symmetry to the statistical mesogen.

We examined the orientation-conformational motion of a molecule subjected to the packing constraints the S_C phase imposes on the molecular motion—stratification together with tilt—by subjecting the primitive mesogen to two conditions. (i) The core segment tends to align along Z', which forms an angle α (not necessarily equal the smectic tilt angle τ) with the layer normal (8). This tendency is dictated by requirements of quasi-parallel packing of the core segments and will be represented by a uniaxial "nematic-like" potential of mean torque

$$V(\theta_0) = -q_0P_2(\cos\theta_0) \qquad (1)$$

where θ_0 is the angle between the core z_0 axis and the Z' axis, q_0 is a strength parameter, and P_2 is the second-rank Legendre polynomial. (ii) The entire mesogen experiences a positional-orientational bias that restricts it within its layer and also tends to prevent the different parts of the same mesogen from violating the "chemical partitioning" within each layer. When averaged over all positions, this bias yields an effective orientational potential V' that necessarily depends on the projection of the mesogen's segments along the smectic layer normal Z. For simplicity we use a form for $V'(R_z)$ that depends on the projection R_z of the primitive mesogen's end-to-end vector **R** along the layer normal Z (Fig. 3) and that tends to suppress the configurations for which either (i) a substantial portion of the mesogen penetrates into the neighboring layers or (ii) the mesogen's projection along Z is small enough to signal severe violation of the intralayer chemical zone boundaries, that is, mixing of cores with tails. We adopt a crude functional form for $V'(R_z)$: All of the configurations for which the magnitude of R_z exceeds a certain upper cutoff value d_u or is smaller than a certain lower cutoff value d_l are rejected and all the configurations with $d_l < |R_z| < d_u$ are accepted with equal weight. This form of the potential introduces a product of two step-function factors, $\Theta(|R_z| - d_l)\Theta(d_u - |R_z|)$ (which equals either 0 or 1), into the orientational distribution function of the molecule, which in effect removes from the space of accessible configurations the ones for which the angle between **R** and the Z axis is below or above the cutoff values $\cos^{-1}(d_u/|\mathbf{R}|)$ or $\cos^{-1}(d_l/|\mathbf{R}|)$, respectively.

With the above specifications of the S_C stratification constraints, the orientational distribution function for the nth conformation of the mesogen is given by

$$f(\omega_0,n) = \zeta^{-1}\, w(n)\, \Theta(|R_z| - d_l)$$
$$\Theta(d_u - |R_z|)\exp[-V(\theta_0)/kT] \qquad (2)$$

where ω_0 denotes the orientation of the core $x_0y_0z_0$ frame relative to the macroscopic XYZ frame, $w(n)$ is the intrinsic weight factor of the nth conformation, ζ is a normalization constant, and kT is the thermal energy. For each conformation, this distribution exhibits the symmetries of the S_C phase, namely it is invariant with respect to twofold rotations about the X axis, it is reflection symmetric with respect to the YZ tilt plane, and it is also inversion symmetric about the intersection of the X axis with the tilt plane. Using this distribution we can evaluate the ensemble average $\langle A\rangle$ of any molecular quantity $A(\omega_0,n)$ according to

$$\langle A\rangle = \Sigma_n \int d\omega_0\, A(\omega_0,n)\, f(\omega_0,n) \qquad (3)$$

The distribution function in Eq. 2, and therefore the averages in Eq. 3, are specified in terms of the parameters α, d_u, d_l, and q^* = q_0/kT. These are, in principle, interdependent (and also temperature-dependent) parameters (9).

We have calculated the relevant order parameters of first rank $C^i_{xX} = \langle\cos(x_i, X)\rangle$ (that is, the averaged cosine of the angle between x_i and X) for the three segments i = 0, 1, 2 in a statistical twofold-symmetric, primitive mesogen—which has identical conformer probabilities $w(n)$—subjected to the S_C stratification constraints given by Eq. 2. (All of the other first-rank order parameters formed from combinations of x_i, y_i, and z_i with X, Y, and Z vanish by symmetry.) The second-rank order parameters $S^i_{ab} = \langle 3\cos(z_i, a)\cos(z_i, b) - \delta_{ab}\rangle/2$, with a, b = X, Y, Z

Table 1. Molecular structures and electric polarizations of ferroelectric liquid crystals. The asterisk indicates a chiral center.

	Primary structure	Polarization (μC m^{-2})	Ref.
I	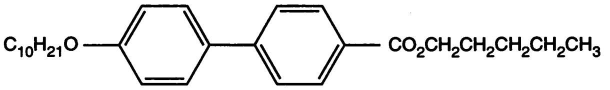	0	(*18*)
II	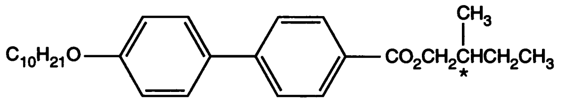	120	(*19*)

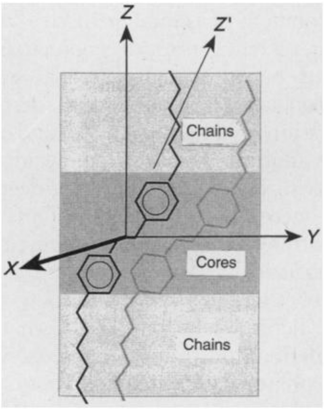

Fig. 1. Mesogens in the monoclinic S_C phase wherein Z' is the axis of preferential alignment and the C_2 axis (X) is normal to the YZ tilt plane, itself a reflection plane having a center of inversion. The latter two symmetry elements are removed when the mesogen is chiral.

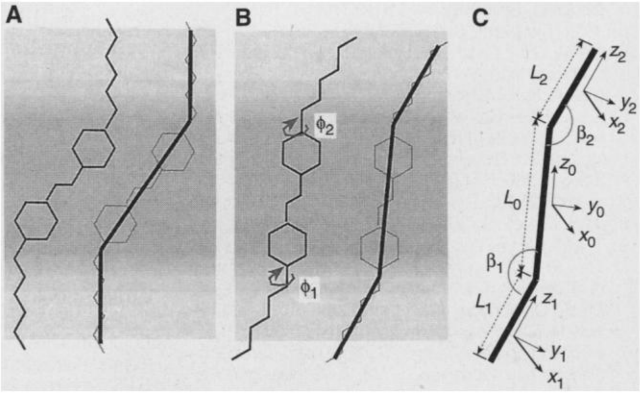

Fig. 2. A primitive mesogen containing one central core segment with two (rigid) tail segments along the mean direction of chain propagation may adopt one of two possible dispositions in a S_C layer: (**A**) the tail direction is tilted less than the core (relative to the layer normal); or (**B**) the tails tilt more than the core. In (**C**) the segments are labeled by i = 0, 1, 2, with 0 referring to the core segment and 1 and 2 referring to the tails, each with lengths denoted by L_i and fixed "valence" angles β_1 and β_2. On each segment a local $x_iy_iz_i$ frame is defined with the z_i axis along the ith segment and the x_i axis normal to the molecular plane.

denoting the axes of the macroscopic frame, were also computed. The results were obtained as functions of the angle α at the fixed value of the strength parameter $q^* = 4$, which yields the appropriate magnitude (~0.75) for the primary order parameter of the core segment in the S_C phase.

Our findings for three representative combinations of the smectic-A zone-thickness parameters d°_u and d°_l (9) are presented for the most symmetric case (*10*) of a primitive mesogen in Fig. 4. The first-rank order parameters $C^1_{xX} = C^2_{xX} \equiv C_{xX}$ of the tail segments in the primitive mesogen are nonvanishing (Fig. 4A), indicating that the ordering of the tail segments relative to the X axis is intrinsically polar in the S_C phase. This is a result of the removal of the statistical twofold rotational symmetry about the primitive mesogen's core z_0 axis through the combined action of the potentials $V(\theta_0)$ and $V'(R_Z)$. This biased correlation of the mesogen's conformation with its orientation applies to both chiral and achiral molecules. The latter have tail segments that are constitutionally symmetric with respect to the y_iz_i plane, that is, the mesogens contain no electrostatic asymmetry with respect to the y_iz_i plane (see compound **I**), and consequently, such achiral (nonpolar) mesogens are mute with respect to the indigenous polarity as it does not contribute to the free energy and will not couple to an external electric field. However, upon the introduction of chirality, with a dipole component along x_i (see compound **II**), a polarization will be obtained: $P_X = N\mu_x C_{xX}$, where N is the number density.

Noteworthy features of the plots in Fig. 4A are the sign of C_{xX} and the trends of its variation with α. In actual S_C phases, an increase in α as a rule corresponds to decreases in the temperature and the layer thickness (*11*). The sign of C_{xX} and its dependence on α are critically affected by d°_u and d°_l. A large d°_u in conjunction with a large d°_l (Fig. 4A, dashed line) yields a negative C_{xX} at small α with an initially increasing magnitude up to a maximum and subsequently decreasing magnitude, eventually undergoing a sign reversal at large α. By contrast, small values of d°_u and d°_l (Fig. 4A, dotted line) give rise to a positive C_{xX} that increases monotonically toward a saturation value. Intermediate d°_u and d°_l values (Fig. 4A, solid line) lead to negative C_{xX} at small α with a subsequent sign reversal and positive growth toward a saturation value. Lastly, the core order parameter C^0_{xX} vanishes if the rotations of the tails about the z_0 axis have twofold symmetry, but it can acquire a nonvanishing value if an a priori asymmetry is introduced by the assignment of different weight factors $w(n)$ to both ϕ_i isomeric states. This is an experimentally testable prediction of the model and suggests that in symmetric molecules, transverse dipoles in the tail are more likely to lead to ferroelectricity than transverse dipoles in the core.

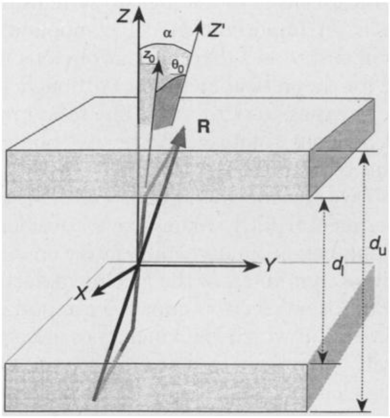

Fig. 3. The end-to-end vector **R** of the primitive mesogen within a smectic layer is indicated relative to the macroscopic *XYZ* frame. *Z'* is the local symmetry axis of the nematic-like potential (tilted at an angle α relative to *Z*) and the core axis z_0 has the orientation θ_0 relative to *Z'*. Physically, d_u is the thickness of an effective layer in which the mesogens are confined.

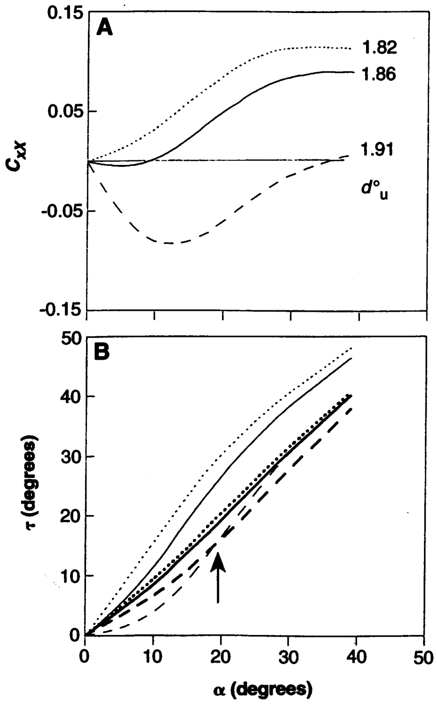

Fig. 4. Predicted behavior of a primitive mesogen subjected to the packing constraints in a smectic. Plots correspond to the following values of d°_u and d°_l (in multiples of the core length L_0): dashed lines, 1.91 and 1.61; solid lines, 1.86 and 1.43; dotted lines, 1.82 and 1.41. **(A)** The order parameter $C_{xX} = \langle \cos(x_i, X) \rangle$ for identical tail segments i = 1, 2 as a function of α. **(B)** The tilt angle τ for the core segment (bold lines) and the tail segments (light lines) as a function of α.

The second-rank order parameters S^i_{XY} and S^i_{XZ} vanish by symmetry. Furthermore, the resulting order tensor for each of the segments *i* can be diagonalized by rotational transformation about the twofold axis X by an angle τ_i to a principal axis frame $X_{(i)}Y_{(i)}Z_{(i)}$ $[X_{(i)} \| X]$ in which the respective order parameter S^i_{YZ} vanishes. These rotations define the tilt angles for the core segment (τ_0) and for the tails ($\tau_1 = \tau_2$) (Fig. 4B). As expected, the removal of the primitive mesogen's statistical twofold symmetry in general causes the different segments to exhibit different principal axes and consequently different tilt angles ($\tau_0 \neq \tau_1$) (*12*). It follows from these plots that those layer-thickness regimes where positive values of C_{xX} are favored correspond to somewhat higher tilt values for the tail segments than for the core (Fig. 2B), whereas the negative polarity regime tends to be associated with the tails less tilted than the core (Fig. 2A). These types of qualitative trends have been observed in the temperature dependence (tilt dependence) of the optical versus x-ray tilt angles and the spontaneous polarization P_X of actual FLC compounds (*13*, *14*). Even the sign variation of P_X exhibited in the plot of C_{xX} versus α (Fig. 4A), behavior reminiscent of the temperature dependence of P_X exhibited by some mesogens (*14*), follows directly from rather simple packing considerations. Here the sign reversal of C_{xX} is a consequence of the shift toward the prevalence of disposition B over A with increasing α.

We infer from our modeling that those attributes of FLCs that have heretofore dominated the discussions of these materials—transverse (average) electric dipoles and their proximity to chiral centers—are necessary only for the purpose of manifesting in a measurable form (spontaneous polarization) an indigenous polar ordering that exists in all tilted smectics. Although previous schematic descriptions of smectic FLCs implicitly acknowledged such polarity (*15*), the focus inevitably was on the chiral and dipolar attributes or "biased rotation" (*4*, *16*) of the rudimentary mesogens. Introducing tilt into smectics spontaneously breaks the statistical symmetry of the mesogen, and because the asymmetry is statistical, it is temperature-dependent. The representation of the tilt and stratification constraints in smectics by potentials of mean torque $V(\theta_0)$ and $V'(R_Z)$ offers a physically well-defined and relatively simple method for understanding how the mesogen's conformational statistics and orientation are biased in the S_C environment. It is tempting, therefore, to use this potential to see how molecular structural modifications of actual mesogens affect ferroelectricity. The calculations presented here for primitive mesogens can be elaborated to include atomistic modeling of actual FLCs, as was demonstrated earlier for nematics (*17*). Then the role of explicit chemical substitutions in hypothetical mesogens subjected to $V(\theta_0)$ and $V'(R_Z)$ can be studied to develop a set of design rules for optimizing spontaneous polarization in FLCs.

REFERENCES AND NOTES

1. R. B. Meyer, presentation at 5th International Liquid Crystal Conference, Stockholm, June 1974; ———, L. Liebert, L. Strzelecki, P. Keller, *J. Phys. Paris Lett.* **36**, 69 (1975); R. B. Meyer, *Mol. Cryst. Liq. Cryst.* **40**, 33 (1977).
2. J. W. Goodby, *Science* **231**, 350 (1986).
3. R. G. Priest, *J. Chem. Phys.* **65**, 408 (1976); see also W. J. A. Goossens, *Phys. Rev. A* **40**, 4019 (1989).
4. D. M. Walba *et al.*, *J. Am. Chem. Soc.* **108**, 5210 (1986).
5. J. S. Patel and J. W. Goodby, *Philos. Mag. Lett.* **55**, 283 (1987).
6. B. Kutnjak-Urbanc and B. Zeks, *Liq. Cryst.* **18**, 483 (1995).
7. Experimental data that could be used to discriminate between dispositions A and B are surprisingly meager [R. Bartolino, J. Doucet, G. Durand, *Ann. Phys. Paris* **3**, 389 (1978); A. Yoshizawa, H. Kikuzaki, M. Fukumasa, *Liq. Cryst.* **18**, 351 (1995)].
8. At this minimal level of modeling, the tails are not subject to a direct orientational bias but are biased indirectly through their attachment to the core.
9. Here we have chosen to treat q^* as an external parameter and to approximate the interdependence between d_u, d_l, and α by the plausible relation $d_{u(l)} = d^\circ_{u(l)} \cos \alpha$, where d°_u and d°_l may be thought of as the respective zone-thickness parameters in the corresponding untilted smectic-A phase.
10. We set $L_1 = L_2 = L$ and $\beta_1 = \beta_2 = \beta$ with $L/L_0 = 0.5$ and $\beta = 145°$ as representative values in the calculations.
11. The tilt $\tau(T) \propto (T_c - T)^\gamma$, where T_c is the smectic-A to smectic-C transition temperature and $\gamma \leq 0.5$ [P. G. de Gennes and J. Prost, *The Physics of Liquid Crystals* (Oxford Univ. Press, Oxford, ed. 2, 1993), p. 527].
12. In a cruder description of orientational averaging in which the stratification constraints are not considered explicitly, each primitive mesogen segment may be thought of as experiencing its own "nematic" orientational potential but with each having a different director orientation. In fact, Priest showed that nonzero polar order parameters are possible using a statistical model of the S_C phase that contains no first-rank interactions that contribute to the orientational order (*3*). His model requires that the relevant second-rank tensorial interactions (minimally two) are diagonal in different frames. However, the specification of different principal frames or directors is introduced in an ad hoc way. In order to rationalize the necessity for different frames or directors and to determine their orientations (their respective tilt angles), one has to resort to stratification constraints of the type we use. Moreover, a nonvanishing C_{xx} can also be obtained even when the tilt angles of the core and the tail segments coincide. An example of this is found in the graphs for $\alpha \approx 20°$, for example, the intersection of the dashed curves in Fig. 4B, marked by an arrow.
13. J. W. Goodby, *Ferroelectric Liquid Crystals* (Gordon and Breach, Amsterdam, 1991), chap. 2.
14. S. Saito *et al.*, *Ferroelectrics* **147**, 367 (1993).
15. P. G de Gennes, *The Physics of Liquid Crystals* (Oxford Univ. Press, Oxford, 2nd printing with additions, 1974), figure 7.18, p. 321; N. A. Clark and S. T. Lagerwall, in (*13*), chap. 1; figure 8 in (*4*). Often the polar order of rigid, monoclinic ("zig zag") mesogens in a monoclinic phase is cached in terms of "biased rotation" about the mesogen's long axis, a mechanism that is frequently invoked in phenomenological descriptions of spontaneous polarization (*4, 16*).
16. K. H. Kim, K. Ishikawa, H. Takezoe, A. Fukuda, *Phys. Rev. E* **51**, 2166 (1995).
17. D. J. Photinos, E. T. Samulski, H. Toriumi, *J. Chem. Phys.* **94**, 2758 (1991); Z. Luz, D. J. Photinos, E. T. Samulski, *J. Am. Chem. Soc.* **115**, 10895 (1993).
18. G. W. Gray and J. W. Goodby, *Mol. Cryst. Liq. Cryst.* **37**, 157 (1976).
19. J. W. Goodby, *J. Mater. Chem.* **1**, 307 (1991); ———, I. Nishiyama, A. J. Slaney, C. J. Booth, K. J. Toyne, *Liq. Cryst.* **14**, 37 (1993).
20. This work was supported by National Science Foundation grant DMR-9412701. D.J.P. acknowledges enlightening discussions with N. Clark and M. Glaser.

11 April 1995; accepted 1 August 1995

Imaging the Electron Density in the Highest Occupied Molecular Orbital of Glycine

Y. Zheng, J. J. Neville, C. E. Brion*

The spherically averaged electron density distribution of the highest occupied molecular orbital (HOMO) for the amino acid glycine has been determined by multichannel electron momentum spectroscopy. Comparison of the measured HOMO electron momentum distribution with near–Hartree-Fock limit and density functional theory (DFT) calculations for the Boltzmann-weighted sum of the eight predicted stable conformers indicates that electron correlation effects must be included in order to adequately reproduce the experimental results for glycine. The best-fitting DFT calculation determined with the Becke-Perdew gradient–corrected exchange-correlation functional was used to generate HOMO electron density maps for oriented glycine conformers. The result is shown for the most stable conformer.

A detailed knowledge of molecular electron density distribution and electron motion is necessary to improve understanding of molecular recognition and chemical reactivity and to facilitate computer-aided molecular design. To date, molecular modeling procedures rely almost exclusively on total charge distributions obtained from molecular potentials. While detailed information on total charge distributions is available from x-ray and electron scattering experiments, the frontier orbital theory of Fukui (*1, 2*) predicts that reactivity is influenced primarily by the electron density distribution in the HOMO. Furthermore, it is clear that chemical behavior is influenced predominantly by the valence electrons. It is therefore highly desirable to obtain accurate experimental measurements of valence orbital electron density distributions. Measurements of orbital electron momentum distributions and thus experimental information on orbital electron density can be obtained for atoms and small molecules (*3–7*) by means of electron momentum spectroscopy (EMS). Recent developments in multichannel EMS (*8, 9*) have provided the increased sensitivity necessary to study larger molecules of interest in biochemistry and molecular biology. Here, we report EMS measurements and quantum mechanical calculations of the HOMO electron density for the amino acid glycine.

Amino acids are of fundamental biochemical interest because of their role as the basic structural units of proteins. Although there is considerable interest in performing electronic structure calculations on proteins, their large molecular size and structural complexity restrict the level at which conventional theoretical methods [that is, Hartree-Frock (HF) and configuration interaction (CI)] can be used in practice. Less computationally intensive theoretical methods such as DFT (*10*) hold considerable promise for use with larger biological molecules. It is of key importance to first test such methods on smaller systems, for which EMS measurements can be made and reasonably high level HF calculations of the HOMO electron distribution and other properties are still possible. As the simplest amino acid, glycine not only has a significant role in biological systems but also is an important model compound in biochemistry and therefore an obvious test case for theoretical methods. Although glycine exists as a zwitterion in the solid phase and aqueous solution, in the gas phase it exists as a mixture of neutral conformers (*11–13*). Recent theoretical (*14–19*) and experimental (*20*) studies have considered the number, geometry, and relative energies of these conformers of the glycine molecule.

EMS is an electron impact ionization experiment, in which the kinematics are completely determined by detecting the two outgoing electrons in coincidence (that is, with time correlation) after energy and angle selection (*3, 5*). The experiment measures spherically averaged electron momentum distributions for individual (binding energy selected) orbitals, that is, orbital imaging in the momentum representation (*3, 5, 7*). According to the plane wave impulse and the target HF approximations (*3, 5, 7*), the EMS

Department of Chemistry, University of British Columbia, Vancouver, BC V6T 1Z1, Canada.

*To whom correspondence should be addressed.